Optimized Carrier-Based DPWM Strategy Adopting Self-Adjusted Redundant Clamping Modes for Vienna Rectifiers With Unbalanced DC Links

Zhijian Zhang, Binxing Li, *Student Member, IEEE*, Guoqiang Zhang, *Senior Member, IEEE*, Gaolin Wang, *Senior Member, IEEE*, Zhaobin Huang, Bin Hu, Tan Long, and Dianguo Xu, *Fellow, IEEE*

***Abstract*—When the Vienna rectifier operates at unbalanced dc links, the conventional carried-based discontinuous pulsewidth modulation (CB-DPWM) strategy suffers from the neutral point (NP) voltage fluctuation and the input current distortion. An optimized CB-DPWM strategy adopting self-adjusted redundant clamping modes is proposed in this article to solve the above issues. To reduce the input current distortion under unbalanced dc links, the modulation waves of CB-DPWM are modified according to the subsector redivision, and the limited operation region can be obtained. To extend the operation range of the Vienna rectifier, the voltage vector trajectory of CB-DPWM is optimized combined with the current error minimization and the voltage loss area compensation. To minimize the NP voltage fluctuation, the redundant clamping modes under unbalanced dc links are self-adjusted in real time according to the unbalanced degree. Moreover, the NP voltage fluctuation of the proposed strategy is evaluated by the root mean square of the NP current fluctuation. The effectiveness of the proposed strategy is verified by experiments on a Vienna rectifier platform.**

***Index Terms*—CB-DPWM, input current distortion, NP voltage fluctuation, self-adjusted redundant clamping modes, unbalanced dc links, Vienna rectifier.**

I. Introduction

COMPARED with the conventional three-level converters, the Vienna rectifier has the advantages of high efficiency, high-power density, and high reliability [1], [2], [3]. In some power conversion applications, the dc-link voltage of the Vienna rectifier can be used as two independent voltage sources to reduce costs [4], [5], [6]. To meet the requirements of the dc-link loads at different working conditions, the voltage sources need to operate at different voltages, resulting in unbalanced dc links of the Vienna rectifier [6]. When the Vienna rectifier operates at unbalanced dc links, the magnitude and the phase of the voltage vector would change, which results in the low-order harmonics of the input currents [7], [8]. In addition, the neutral point (NP) voltage of conventional pulsewidth modulation (PWM) has three times grid frequency fluctuation, which affects the power quality of the dc link of the Vienna rectifier [9], [10]. Therefore, the advanced control and modulation method for Vienna rectifier with unbalanced dc links needs further investigation.

To reduce input current distortion under unbalanced dc links, the effect of voltage vector change on the voltage synthesis should be considered. The strategies can be generally classified into two groups: the space-vector PWM (SVPWM) strategies and the carrier-based pulsewidth modulation (CB-PWM) strategies [11], [12], [13]. For the SVPWM strategies, a new SVPWM strategy was proposed in [14], which can reduce the low-frequency output voltage distortion. In [15], a modified SVPWM strategy was proposed to optimize the subsector division. In order to reduce the computational burden, a redundant vector preselection optimal switching sequence model predictive control scheme was proposed in [16]. Compared with the SVPWM strategies, the CBPWM-based strategies are simple to implement. A simplified PWM strategy was proposed in [17], which omits to detect the position of the reference voltage vector and maximizes the linear modulation range. In [18], a hybrid PWM strategy combined the SVPWM and CB-PWM method was proposed, which can realize the asymmetric control of the dc-link voltages. However, the above CB-PWM-based strategies are mainly aimed at the three-level neutral-point clamped converter and lead to the input current distortion at zero-crossing point due to violating the basic rule of the Vienna rectifier [19]. In [20], a modified CB-PWM was proposed to reduce the low-order harmonics of the input currents for the Vienna rectifier. In [21], a novel zero-sequence component injection modulation method was proposed to improve the input current quality of the Vienna rectifier with unbalanced dc-link voltages.

To reduce the NP voltage fluctuation with unbalanced dc links, the NP current fluctuation should be suppressed. In [22], an improved virtual space vector pulsewidth modulation (VSVPWM) was proposed to eliminate the fluctuation of the NP voltage. In [23], the virtual space-vector diagram (VSVD) with unbalanced dc links was proven identical to the VSVD with balanced dc

Manuscript received 13 June 2022; revised 15 August 2022; accepted 28 September 2022. Date of publication 5 October 2022; date of current version 18 November 2022. This work was supported by the Research Fund for the National Natural Science Foundation of China under Grant 52125701, Grant 52207042, Grant 52177034. Recommended for publication by Associate Editor L. Wang. *(Corresponding author: Binxing Li.)*

Zhijian Zhang, Binxing Li, Guoqiang Zhang, Gaolin Wang, and Dianguo Xu are with the School of Electrical Engineering and Automation, Harbin Institute of Technology, Harbin 150001, China (e-mail: 21b906027@stu.hit.edu.cn; li_binxing@163.com; zhgq@hit.edu.cn; wgl818@hit.edu.cn; xudiang@hit.edu.cn).

Zhaobin Huang, Bin Hu, and Tan Long are with the Guangdong Midea Air-Conditioning Equipment Co., Ltd., Foshan, Guangdong 528311, China (e-mail: zhaobin.huang@midea.com; hubin13@midea.com; longtan1@midea.com).

Color versions of one or more figures in this article are available at https://doi.org/10.1109/TPEL.2022.3212072.

Digital Object Identifier 10.1109/TPEL.2022.3212072

links. However, the VSVPWM strategy is not suitable for the Vienna rectifier due to the disabling of small vectors in one sector. In order to meet the basic rule of the Vienna rectifier, a novel CB-PWM with segmented component was proposed to reduce the NP current fluctuation and the input current distortion under balanced and unbalanced dc links [4].

The above strategies belong to the continuous PWM, and it is recommended to adopt the discontinuous PWM (DPWM) strategies to improve the efficiency and the power density of the Vienna rectifier [24], [25]. In [26], an adaptive control of DPWM was proposed to reduce the input current distortion under unbalanced dc links. In [27], an analytical DPWM was proposed, which can suppress output harmonics and maximize the linear modulation region. However, when the above strategies are adopted, the output voltage of Vienna rectifier and the input current directions are opposite in some regions, which adds the harmonics of the input current. For the Vienna rectifier, a dynamic space vector DPWM was proposed to eliminate the effect of the deviation vector, reducing the input current distortion [28]. However, the vector diagram with unbalanced dc-link voltages is asymmetric and complicated. In [29], a hybrid carrier-based discontinuous PWM (CB-DPWM) scheme was proposed, which can reduce the input current harmonics by injecting modified zero sequence components. Based on the above-mentioned analysis, the CB-DWPM can reduce the computational burden and the input current distortion by modifying the zero sequence components. However, the NP voltage fluctuation of conventional CB-DPWM strategies still exists. In addition, the CB-DPWM has limited operation regions under unbalanced dc links. As a result, the CB-DPWM strategy for Vienna rectifiers with unbalanced dc links needs further research.

This article proposes an optimized carrier-based DPWM strategy adopting the self-adjusted redundant clamping modes for Vienna rectifiers with unbalanced dc links. First, the limited operation regions and the NP voltage fluctuation of the conventional CB-DPWM strategy are analyzed. To extend the operation range of the Vienna rectifier, the voltage vector trajectory of the conventional CB-DPWM strategy is optimized by the current error minimization and the voltage loss area compensation, which can improve the fundamental amplitude of the output voltage and reduce the input current harmonics. Then, the redundancy clamping modes under unbalanced dc links are analyzed and self-adjusted based on the unbalanced degree to suppress the NP voltage fluctuation. Finally, experiments are performed on a Vienna rectifier platform to validate the effectiveness of the proposed strategy.

II. Analysis of Conventional CB-DPWM Strategy for Vienna Rectifiers With Unbalanced DC Links

A. Operation Region of Conventional CB-DPWM Strategy

Fig. 1 shows the typical topology of the Vienna rectifier. The PO and ON of the dc link are connected to different loads, respectively. To meet the different power requirements of the loads, the dc-link voltages should be different.

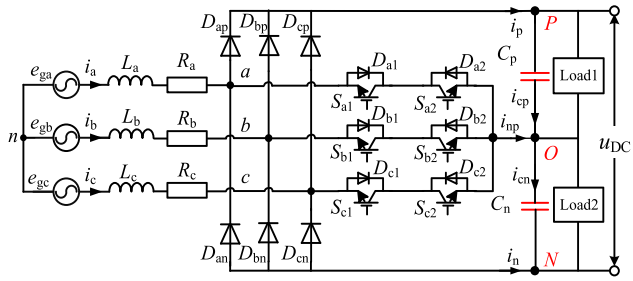

Fig. 1. Typical topology of the Vienna rectifier.

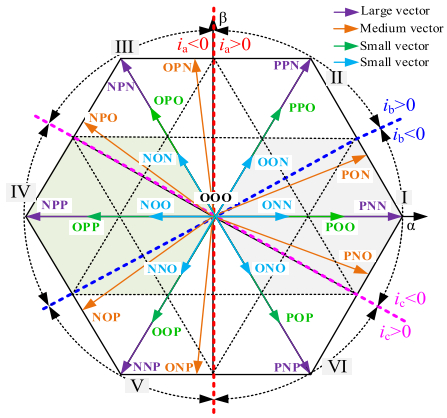

Fig. 2. Vector diagram with unbalanced dc-links.

To describe the difference of the dc output voltage, the unbalance degree δ is defined as

$$\delta = \frac{u_{\mathrm{PO}} - u_{\mathrm{ON}}}{u_{\mathrm{DC}}} \tag{1}$$

where u_{PO}, u_{ON}, and u_{DC} are the voltages of the top and bottom dc-link capacitors, and the dc-link voltage, respectively.

When $\delta > 0$, the vector diagram with unbalanced dc links is shown in Fig. 2, which is not affected by the lag grid currents. As can be seen that in sector I, the large vectors PNN and the zero vectors OOO are not affected by unbalanced dc links. However, the magnitudes of the small vectors POO and ONN are different, which leads to the error of the voltage synthesis. Therefore, it needs to redistribute the duty cycles of the voltage vector. Since the zero-crossing point of the input current remains unchanged, such as $i_{\mathrm{b}} = 0$, the sector division of unbalanced dc links is the same as that of balanced dc links. However, due to the position change of the medium vectors, such as PON and PNO, the subsectors need to be redivided. In particular, it is always disabled to output two large vectors in one sector for the Vienna rectifiers due to the force-commutated current.

Due to the symmetry, the sector I is taken as an example to analyze. In sector I, when $\delta > 0$, two subsector division methods are shown in Fig. 3. One of the subsectors division methods is divided with the small vector POO as the center, which is defined as DPWMMAX. The other is centered on the small vector ONN, which is defined as DPWMMIN.

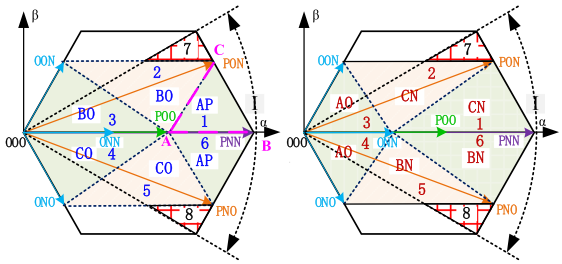

Fig. 3. Two subsector division methods of the sector I. (a) DPWMMAX. (b) DPWMMIN.

TABLE I
JUDGMENT CONDITIONS AND INJECTED ZERO SEQUENCE COMPONENTS OF DPWMMAX

Subsector	Judgment condition	Injected zero sequence component
1	$u_{ra} > u_{rb}+u_{PO} > u_{rc}+u_{PO}$	$-u_{ra}+u_{PO}$
2	$u_{rb}+u_{PO} > u_{ra} > u_{rc}+u_{PO}$	$-u_{rb}$
3	$u_{rb}+u_{PO} > u_{rc}+u_{PO} > u_{ra}$	$-u_{rb}$
4	$u_{rc}+u_{PO} > u_{rb}+u_{PO} > u_{ra}$	$-u_{rc}$
5	$u_{rc}+u_{PO} > u_{ra} > u_{rb}+u_{PO}$	$-u_{rc}$
6	$u_{ra} > u_{rc}+u_{PO} > u_{rb}+u_{PO}$	$-u_{ra}+u_{PO}$

The judgment condition of the DPWMMAX subsector 1 as shown in Fig. 3(a) is taken as an example to illustrate. Subsector 1 is surrounded by the AB and AC vectors. The β-axis component of the vector AB is zero. The expression of the vector ac satisfies

$$u_{r\beta 1} = \sqrt{3}\left(u_{r\alpha 1} - \frac{2}{3}u_{PO}\right) \tag{2}$$

where $u_{r\alpha 1}$ and $u_{r\beta 1}$ are the $\alpha\beta$-axis components of the vector ac, respectively. The three-phase reference voltage in the $\alpha\beta$-axis can be obtained as

$$\begin{cases} u_{r\alpha} = (2u_{ra} - u_{rb} - u_{rc})/3 \\ u_{r\beta} = \sqrt{3}(u_{rb} - u_{rc})/3 \end{cases} \tag{3}$$

where u_{rx} (x = a, b, and c) is the three-phase reference voltage, $u_{r\alpha}$ and $u_{r\beta}$ are the $\alpha\beta$-axis voltage of the reference voltage. According to (2) and (3), the judgment condition of the subsector 1 is

$$u_{ra} > u_{rb} + u_{PO} > u_{rc} + u_{PO}. \tag{4}$$

According to Fig. 3(a), the reference voltage of subsector 1 is synthesized by the voltage vectors POO, PON, and PNN. The a-phase voltage is clamped to the P state, meaning that the a-phase output voltage is u_{PO}. Therefore, the injected zero sequence component of DPWMMAX subsector 1 is

$$u_{com} = -u_{ra} + u_{PO}. \tag{5}$$

The judgment conditions and injected zero sequence components of DPWMMAX are shown in Table I.

To simplify the injected zero sequence component of DPWMMAX, the new modulation wave is defined as

$$w_{x1} = \begin{cases} u_{rx\_per} & u_{rx\_per} \geq 0 \\ u_{rx\_per} + 1 + \delta & u_{rx\_per} < 0 \end{cases} \tag{6}$$

where u_{rx_per} is the normalized references voltage by $u_{DC}/2$, which can be expressed as

$$\begin{cases} u_{ra\_per} = m\cos\theta \\ u_{rb\_per} = m\cos(\theta - 2\pi/3) \\ u_{rc\_per} = m\cos(\theta + 2\pi/3) \end{cases} \tag{7}$$

where θ is the angle of the reference voltage vector, and m is the modulation index.

Therefore, according to Table I and (6), the injected zero sequence component of DPWMMAX under unbalanced dc links can be uniformly written as

$$u_{com1} = 1 + \delta - w_{max\,1} \tag{8}$$

where $w_{max\ 1}$ is the maximum w_{x1}.

When the range of the carrier is $[-1, 1]$, the modulation wave of DPWMMAX under unbalanced dc links is

$$u_{x\_DPWMMAX} = \frac{u_{rx\_per} + u_{com1}}{1 + \mathrm{sgn}(i_x)\,\delta}. \tag{9}$$

Similarly, the injected zero sequence component of DPWMMIN can be written as

$$u_{com2} = -w_{min\,2} \tag{10}$$

where $w_{min\ 2}$ is the minimum w_{x2}, which is defined as

$$w_{x2} = \begin{cases} u_{rx\_per} & u_{rx\_per} \geq 0 \\ u_{rx\_per} + 1 - \delta & u_{rx\_per} < 0. \end{cases} \tag{11}$$

The modulation wave of DPWMMIN under unbalanced dc links is

$$u_{x\_DPWMMIN} = \frac{u_{rx\_per} + u_{com2}}{1 + \mathrm{sgn}(i_x)\,\delta}. \tag{12}$$

In order to simplify the modulation wave of DPWM under unbalanced dc links, (9) and (12) can be uniformly written as

$$u_{x\_DPWM} = \frac{u_{rx\_per} + u_{com}}{1 + \mathrm{sgn}(i_x)\,\delta} \tag{13}$$

where u_{com} is the injected zero sequence component of DPWM, which can be defined as

$$u_{com} = k_c(1 + \delta - w_{max\,1} + w_{min\,2}) - w_{min\,2} \tag{14}$$

where k_c is the switching coefficient. If $k_c = 1$, the modulation wave is selected as DPWMMAX. If $k_c = 0$, the modulation wave is selected as DPWMMIN.

As can be seen from (13), the modulation wave of DPWM can be implemented without detecting the position of the reference voltage vector and reduce the low-order harmonics due to considering the effect of the voltage vectors changes.

However, when the dc-link voltages are unbalanced, the reference voltage cannot be synthesized in some regions due to the changes of the voltage vectors. Considering that the ratio of the inductance voltage drop in the grid voltage is small, the input current is basically in phase with the grid voltage when the power

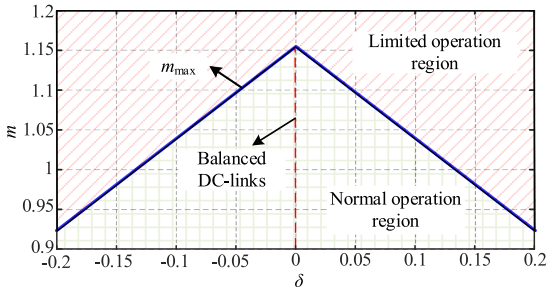

Fig. 4. Limited operation region and normal operation region.

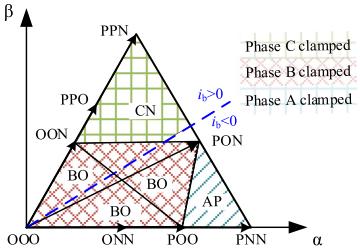

Fig. 5. Clamping modes of the conventional CB-DPWM strategy.

factor is equal to 1. In Fig. 3(a), the available vectors PON, OON, ONO, and PNO in sector I cannot completely cover [-π/6, π/6]. When $\delta > 0$, the voltage vectors of subsectors 7 and 8 called nonsynthetic subsectors cannot be synthesized, which limits m of the reference voltage. The maximum m under unbalanced dc links could be calculated by

$$m_{\max}=\frac{2}{\sqrt{3}}\left(1-|\delta|\right). \tag{15}$$

When $\delta < 0$, the $m_{\max}$ is the same as (15). When $m > m_{\max}$, it is defined as the limited operation region. When $m < m_{\max}$, it is defined as the normal operation region. From (15), the limited operation region and the normal operation region can be obtained, as shown in Fig. 4. The normal operation region is symmetric about $\delta = 0$. When $\delta = 0$, $m_{\max} = 1.15$, and the rectifier can operate the whole linear region. With the increase of δ, the normal operation region becomes smaller, and the limited operation region becomes larger. As a result, the normal operation region of the conventional DPWM strategy is limited by the unbalanced degree.

B. Analysis of NP Voltage Fluctuation

The unbalanced dc links not only limit the normal operation region of the conventional CB-DPWM strategy, but also cause NP voltage fluctuation. To ensure the normal operation of the Vienna rectifier and reduce the switching loss, $k_c = 1$ at the sectors I, III, and V and $k_c = 0$ at the sectors II, IV, and VI are adopted by the conventional CB-DPWM strategy [29]. In [0, π/3], clamping modes of the conventional CB-DPWM strategy are shown in Fig. 5.

To analyze the NP voltage fluctuation of the conventional CB-DPWM strategy, the intervals [0, π/3] can be divided into three regions: AP, BO, and CN. When the reference voltage is

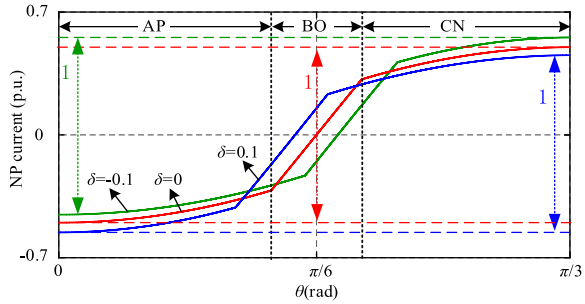

Fig. 6. NP currents with different δ.

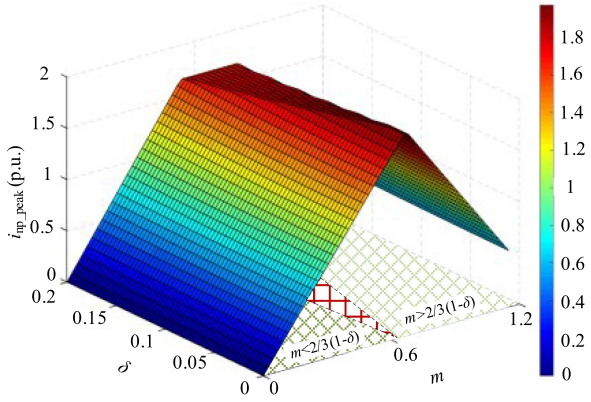

Fig. 7. Peak-to-peak values of the NP current under different m and δ.

in the AP, the duty cycles of the three-phase voltages can be expressed as

$$\begin{cases} d_a = 0 \\ d_b = \frac{u_{rb\_per}-u_{ra\_per}+2}{1-\delta} \\ d_c = \frac{u_{rc\_per}-u_{ra\_per}+2}{1-\delta}. \end{cases} \tag{16}$$

The NP current of the AP region can be obtained as

$$i_{np} = \frac{u_{ra\_per}i_a + u_{rb\_per}i_b + u_{rc\_per}i_c - 2i_a}{1-\delta}. \tag{17}$$

Using (17), the NP currents with different δ can be obtained as shown in Fig. 6. When $\theta = 0$, the NP current is the minimum, and when $\theta = \pi/3$, the NP current is the maximum. The peak-to-peak values of the NP currents with different δ are the same, which are equal to 1. Therefore, to illustrate the fluctuation of the NP current, the peak-to-peak value of the NP current can be used, which is defined as

$$i_{np\_peak} = \frac{i_{np\_max} - i_{np\_min}}{I_m} \tag{18}$$

where i_{np_max} and i_{np_min} are the maximum and minimum values of the NP current, respectively, and I_m is the amplitude of the input current.

Fig. 7 shows the peak-to-peak values of the NP current under different m and δ. It can be seen that i_{np_peak} of the conventional DPWM strategy is unrelated to δ. When $m \neq 0$, there is the NP current fluctuation, which reaches the maximum at $2(1-\delta)/3 < m < 2(1+\delta)/3$. Therefore, the NP voltage fluctuation of the Vienna

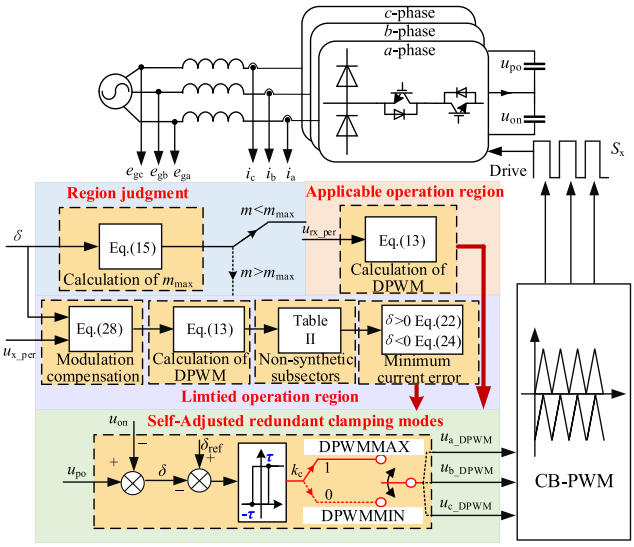

Fig. 8. Block diagram of the proposed CB-DPWM strategy.

TABLE II
JUDGMENT CONDITIONS OF THE NONSYNTHETIC SUBSECTORS

Sector	Judgment condition
I, III, V	u_{min_per}<-1|| u_{mid_per}>0||u_{max_per}>1
II, IV, VI	u_{min_per}<-1|| u_{mid_per}<0||u_{max_per}>1

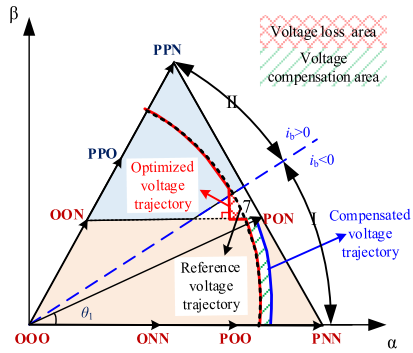

Fig. 9. Optimization of the DPWM voltage vector trajectory.

rectifier cannot be suppressed by the conventional CB-DPWM strategy.

III. Optimized CB-DPWM Strategy With Self-Adjusted Redundant Clamping Modes

A. Scheme of Proposed CB-DPWM Strategy

To extend the operation range and reduce the NP voltage fluctuation of the Vienna rectifier with unbalanced dc links, an optimized CB-DPWM strategy adopting self-adjusted redundant clamping modes is proposed, whose block diagram is shown in Fig. 8. It includes four parts: the region judgment, the self-adjusted redundant clamping modes, the DPWM calculation of the normal operation region, and the DPWM calculation of the limited operation region.

First, $m_{\max}$ is calculated by (15). When $m < m_{\max}$, the reference voltage is in the normal operation region. The DPWM modulation wave can be obtained according to (13) and reduce the low-order harmonics of the input current. When $m > m_{\max}$, the reference voltage is in the limited operation region. The voltage vector trajectory of the DPWM is optimized with the current error minimization and the voltage loss area compensation to extend the operation range. Based on the DPWM modulation wave, the redundant clamping modes can be real-time self-adjusted according to the unbalanced degree, which can effectively reduce the NP voltage fluctuation.

B. Optimization of Voltage Vector Trajectory for DPWM

From the above analysis, when $m > m_{\max}$, there are nonsynthetic subsectors in the vector diagram, where the modulation wave will overmodulate or violate the Vienna rectifier's basic rules. To extend the operation range of the Vienna rectifier, the voltage vector trajectory of DPWM needs to be optimized.

First, judgment conditions of the nonsynthetic subsectors are shown in Table II, where $u_{\min\_per}$, $u_{\mathrm{mid\_per}}$, and $u_{\max\_per}$ are minimum, middle, and maximum of DPWM modulation waves $u_{\mathrm{x\_DPWM}}$, respectively.

To facilitate the analysis, the intervals [0, π/3] are taken as an example to illustrate the optimization of the DPWM voltage vector trajectory, as shown in Fig. 9. When the reference voltage is in sector I, the maximum region is surrounded by the voltage vectors OOO, PNN, PON, and OON. When the reference voltage is in the nonsynthetic subsector 7, the voltage-second balance principle cannot be satisfied. To reduce the voltage vector error, OON and PON can be used to synthesize the reference voltages in the nonsynthetic subsector 7.

The dwell times of OON and PON are defined hT_{s} and $(1\text{-}h)T_{\mathrm{s}}$, respectively. The current vector error in a switching cycle is

$$\begin{cases} \Delta i_\alpha = \frac{u_{\mathrm{OON}\_\alpha}-u_{\mathrm{r}\alpha}}{L} hT_{\mathrm{s}} + \frac{u_{\mathrm{PON}\_\alpha}-u_{\mathrm{r}\alpha}}{L}(1-h)T_{\mathrm{s}} \\ \Delta i_\beta = \frac{u_{\mathrm{OON}\_\beta}-u_{\mathrm{r}\beta}}{L} hT_{\mathrm{s}} + \frac{u_{\mathrm{PON}\_\beta}-u_{\mathrm{r}\beta}}{L}(1-h)T_{\mathrm{s}} \end{cases} \tag{19}$$

where u_{OON_α} and u_{OON_β} are the $\alpha\beta$-axis voltage of OON, and u_{PON_α} and u_{PON_β} are the $\alpha\beta$-axis voltage of PON, respectively.

According to (19), the module of the current vector is

$$|\Delta \boldsymbol{i}| = \sqrt{(\Delta i_\alpha)^2 + (\Delta i_\beta)^2}. \tag{20}$$

The minimum of the current vector error can be obtained by calculating the derivative of $|\Delta \boldsymbol{i}|$. When the derivative is zero, h can be expressed as

$$h = \frac{3+\delta-3u_{\mathrm{rmax\_per}}}{2(1+\delta)} \tag{21}$$

where $u_{\mathrm{rmax\_per}}$ is the maximum of $u_{\mathrm{rx\_per}}$. The modulation wave of the nonsynthetic subsectors can be obtained as

$$\begin{cases} u_{\mathrm{max\_per}} = 1-h \\ u_{\mathrm{mid\_per}} = 0 \\ u_{\mathrm{min\_per}} = -1. \end{cases} \tag{22}$$

Similarly, when $\delta < 0$, h of the nonsynthetic subsectors is

$$h = \frac{3 - \delta + 3u_{\text{min\_per}}}{2(1-\delta)}. \tag{23}$$

The corresponding modulation wave of the nonsynthetic subsectors can be obtained as

$$\begin{cases} u_{\text{max\_per}} = 1 \\ u_{\text{mid\_per}} = 0 \\ u_{\text{min\_per}} = -1 + h. \end{cases} \tag{24}$$

The optimized voltage vector trajectory as shown in Fig. 9 is equivalent to the reference voltage vector making a vertical on the available vector PON and OON connection line, which is minimum error of the current vector. However, due to the loss area of voltage, the fundamental amplitude of the fundamental voltage is reduced.

To improve the fundamental amplitude of the output voltage, the modulation compensation is introduced. The loss area of the optimized voltage is shown in the red shaded part of Fig. 9. To reduce the voltage loss area, the voltage compensation area is shown in the green shaded part of Fig. 9.

To simplify the calculation, the voltage loss area and the voltage compensation area are approximated as the triangle and the parallelogram, respectively. When the two areas are equal, the result can be obtained

$$(|\boldsymbol{u}_{\text{com}}| - |\boldsymbol{u}_{\text{ref}}|)\, u_{\text{PON\_}\beta} = \frac{(|\boldsymbol{u}_{\text{ref}}| - 2u_{\text{PON\_}\beta})^2}{8\sqrt{3}} \tag{25}$$

where $|\boldsymbol{u}_{\text{com}}|$ and $|\boldsymbol{u}_{\text{ref}}|$ are the magnitudes of the compensation voltage vector and the reference voltage vector, respectively. Solving (25), the added modulation index can be derived as

$$m_{\text{add}} = \frac{\left[m - \frac{2}{\sqrt{3}}(1-\delta)\right]^2}{8(1-\delta)}. \tag{26}$$

As can be seen from Fig. 2, when $\delta > 0$, the reference voltage at sectors I, III, and V needs compensation. Similarly, when $\delta < 0$, the reference voltage at sectors II, IV, and VI needs compensation, and the added modulation index can be expressed as

$$m_{\text{add}} = \frac{3\left(m - \frac{2}{3}(1+\delta)\right)^2}{8(1+\delta)}. \tag{27}$$

Then, the three-phase reference voltage with the voltage loss area compensation can be expressed as

$$u_{\text{x\_per}} = \frac{m + m_{\text{add}}}{m} u_{\text{rx\_per}} \tag{28}$$

where $u_{\text{x\_per}}$ is the sinusoidal references voltage in the limited operation region.

With the voltage vector trajectory optimization, the modulation waves of DPWM when $m = 1.15$ and $\delta = 0.2$ are shown in Fig. 10. From Fig. 10(a), the conventional DPWM has overmodulation in the BO clamping interval, and its fundamental amplitude is 1.14, which is lower than m. In Fig. 10(b), the optimized DPWM can ensure that there is no overmodulation in the BO clamping interval, and the output fundamental amplitude is 1.15 that is equal to m.

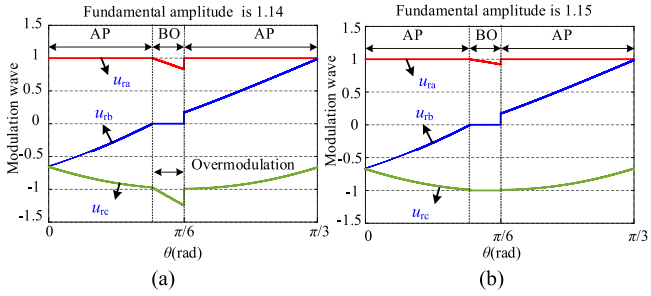

Fig. 10. Modulation wave of DPWM. (a) Conventional DPWM. (b) Optimized DPWM.

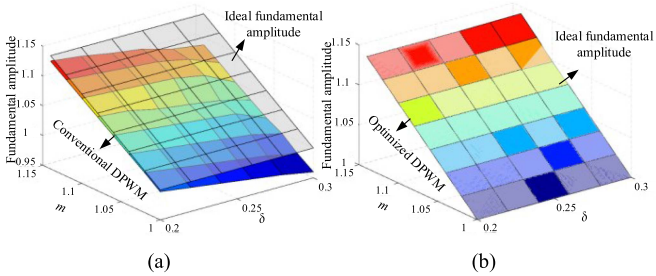

Fig. 11. Comparison of the conventional and optimized DPWM fundamental amplitude. (a) Conventional DPWM. (b) Optimized DPWM.

The comparison between the conventional and optimized DPWM fundamental amplitude of the output voltage is shown in Fig. 11. As can be seen from Fig. 11(a), the fundamental amplitude of the conventional DPWM cannot be equal to m due to the existence of the nonsynthetic subsectors. With the increase of δ, the fundamental amplitude of the conventional DPWM output voltage decreases, which limits the operation range of Vienna rectifier. In Fig. 11(b), the fundamental amplitude of the optimized DPWM is basically the same as m, regardless of the change of δ. Therefore, by optimizing the voltage vector trajectory of DPWM, the fundamental amplitude of the output voltage can be increased, which can extend the operation range of the Vienna rectifier.

Fig. 12 shows the modulation waves of the reference voltage under different m and δ. From Fig. 12, the modulation waves exist the limited operation interval when $m > m_{\max}$, which is proportional to m and δ. In the limited operation interval, the reference voltage vector is synthesized by the voltage vectors PON and OON, and b-phase and c-phase voltage are clamped to 0 and -1, respectively. As a result, the ranges of the three-phase reference voltages are [0, 1], which avoids the overmodulation and ensures the normal operation of the Vienna rectifier.

C. Self-Adjusted Redundancy Clamping Modes

The voltage vector trajectory optimization of DPWM can extend the operation range of the Vienna rectifier, but the NP voltage fluctuation is not suppressed. To minimize the NP voltage fluctuation, the redundant clamping modes are obtained under unbalanced dc links. Two different clamping modes have

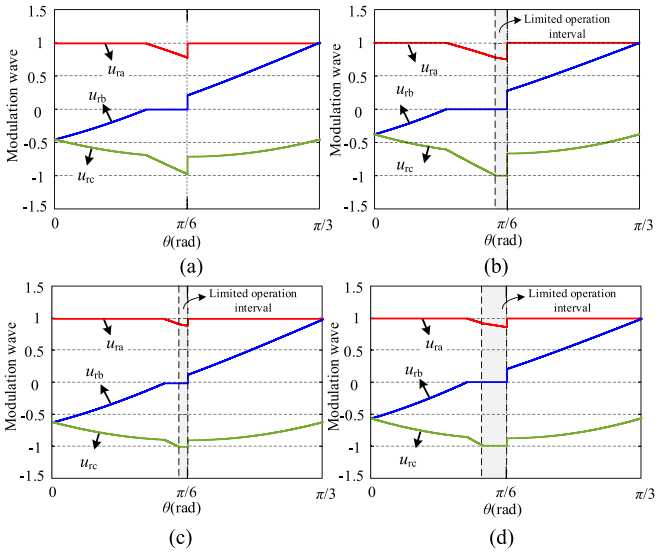

Fig. 12. Modulation waves of the reference voltage under different m and δ. (a) $m = 1$ and $\delta = 0.1$. (b) $m = 1$ and $\delta = 0.2$. (c) $m = 1.1$ and $\delta = 0.1$. (d) $m = 1.1$ and $\delta = 0.2$.

opposite effects on the NP voltage with the same voltage vector, which are called the redundant clamping modes.

To obtain the redundant clamping modes under the unbalanced dc links, the NP current in [0, π/3] is first obtained

$$i_{\mathrm{np}} = -\sum_{\mathrm{x=a,b,c}} \frac{u_{\mathrm{rx\_per}}}{1+\mathrm{sgn}(i_{\mathrm{x}})\delta} |i_{\mathrm{x}}| - u_{\mathrm{com}} \left(\frac{i_{\mathrm{a}}}{1+\delta} + \frac{|i_{\mathrm{b}}|}{1+\mathrm{sgn}(i_{\mathrm{b}})\delta} - \frac{i_{\mathrm{c}}}{1-\delta} \right). \tag{29}$$

From (29), the NP current mainly depends on the injected zero sequence component u_{com} with the same δ and is inversely proportional to u_{com}. Since the redundant clamping modes mainly depends on the NP current, the clamping modes corresponding to the maximum and minimum NP currents are analyzed.

When the reference voltage is located at subsector 1 as shown in Fig. 3(a), to ensure normal operation of the Vienna rectifier, the following inequalities need to be satisfied:

$$\begin{cases} 0 \le u_{\mathrm{ra\_per}} + u_{\mathrm{com}} \le 1 + \delta \\ \delta - 1 \le u_{\mathrm{rb\_per}} + u_{\mathrm{com}} \le 0 \\ \delta - 1 \le u_{\mathrm{rc\_per}} + u_{\mathrm{com}} \le 0. \end{cases} \tag{30}$$

According to (4) and (30), the range of u_{com} can be written as

$$\delta - 1 - u_{\mathrm{rc\_per}} \le u_{\mathrm{com}} \le 1 + \delta - u_{\mathrm{ra\_per}}. \tag{31}$$

The maximum of u_{com} is equivalent to clamping the a-phase voltage to the P state, where the NP current is the minimum. The minimum of u_{com} is equivalent to the c-phase voltage clamping to the N state, where the NP current is the maximum. The clamping modes corresponding to the maximum and minimum NP currents in [0, π/3] are shown in Fig. 13. The red clamping modes represent the minimum NP current, which are the same as the clamping modes corresponding to $k_{\mathrm{c}} = 1$. The black clamping modes represent the maximum NP current, which are the same as the clamping modes corresponding to $k_{\mathrm{c}} = 0$. Therefore, when the voltage vector is synthesized, the NP current is the minimum with $k_{\mathrm{c}} = 1$ and the maximum with $k_{\mathrm{c}} = 0$.

The NP current of DPWM under different m and δ conditions is shown in Fig. 14. In Fig. 14(a), when the reference voltage is in the normal operation region, the NP current of $k_{\mathrm{c}} = 0$ is greater than 0, thereby increasing the NP voltage. In Fig. 14(b), the NP current of $k_{\mathrm{c}} = 1$ is greater than 0 in some regions, which are inversely proportional to δ. When $\delta = 0.133$, the intervals where the NP current is greater than 0 reach the maximum and are 5% of the whole regions. Therefore, the NP current of $k_{\mathrm{c}} = 1$ is basically less than zero in [0, π/3], and the NP voltage can be reduced. From Fig. 14(c), when the reference voltage is in the normal operation region, the NP current of $k_{\mathrm{c}} = 0$ is greater than 0 and is unrelated to m. The NP voltage can be increased with $k_{\mathrm{c}} = 0$. In Fig. 14(d), the NP current of $k_{\mathrm{c}} = 1$ is greater than zero in some regions, which are 3% of the whole regions. Therefore, the NP current of $k_{\mathrm{c}} = 1$ is approximately less than 0, thereby reducing the NP voltage.

In the normal operation region, the clamping modes corresponding to $k_{\mathrm{c}} = 1$ and $k_{\mathrm{c}} = 0$ have opposite effects on the NP voltage, which are redundant clamping modes. To realize the suppression of the NP voltage fluctuation, the self-adjusted redundant clamping modes as shown in Fig. 8 are proposed. δ_{ref} is the reference unbalance degree and τ is the allowable NP voltage fluctuation. From Fig. 8, k_{c} is mainly depended on the output of the hysteresis control. When $\delta_{\mathrm{ref}} > \delta+\tau$, the hysteresis control reaches the upper limit, and δ should be increased at this time. When $k_{\mathrm{c}} = 1$, the NP current is basically less than 0, which can increase u_{PO} and reduce u_{ON}. As a result, δ is increased. Similarly, when $\delta_{\mathrm{ref}} < \delta+\tau$, the hysteresis control reaches the lower limit, and k_{c} is equal to zero. When $k_{\mathrm{c}} = 0$, the NP current is greater than zero, and δ is decreased.

When the unbalance degree is in [-τ, τ], the voltage difference between the top and bottom dc-link capacitors meets

$$-\tau u_{\mathrm{DC}} \le \Delta u \le \tau u_{\mathrm{DC}}. \tag{32}$$

It can be seen that Δu can be reduced by changing τ. Therefore, when the reference voltage is in the normal operation region, the NP voltage fluctuation can be suppressed by the self-adjusting redundant clamping modes. However, when the reference voltage is in the limited operation region, it is necessary to further analyze the NP voltage fluctuation of the proposed strategy.

When $m = 1.15$ and $\delta = 0.2$, NP currents corresponding to $k_{\mathrm{c}} = 0$ and $k_{\mathrm{c}} = 1$ are shown in Fig. 15. It is mainly divided into three regions: the bidirectional control region (BCR), the unidirectional control region (UCR), and the uncontrollable region (UR). When the NP currents of $k_{\mathrm{c}} = 0$ and $k_{\mathrm{c}} = 1$ are respectively larger and less than zero, the bidirectional control of the NP voltage can be realized, which is called BCR. In BCR, the proposed strategy can suppress NP voltage fluctuation by the self-adjusting redundant clamping modes. When the NP currents of $k_{\mathrm{c}} = 0$ and $k_{\mathrm{c}} = 1$ are both larger or less than zero, the unidirectional control of the NP voltage can be realized, which is called UCR. In UCR, the changing rate of the NP voltage is adjustable with the redundant clamping modes, and there is NP

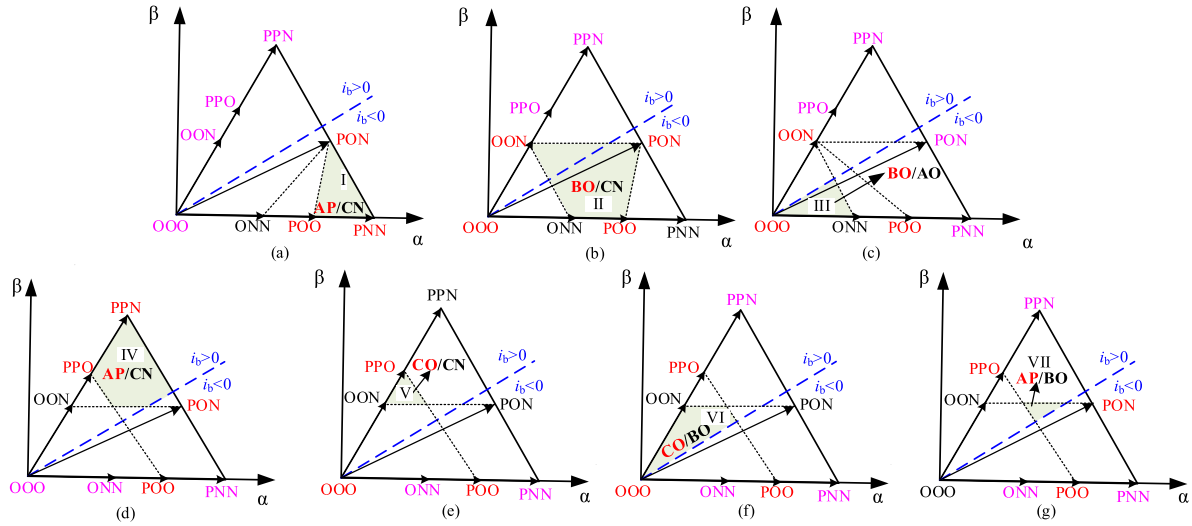

Fig. 13. Clamping mode corresponding to the maximum and minimum NP currents in [0, π/3]. (a) Subsector I. (b) Subsector II. (c) Subsector III. (d) Subsector IV. (e) Clamping mode of subsector V. (f) Clamping mode of subsector VI. (g) Clamping mode of subsector VII.

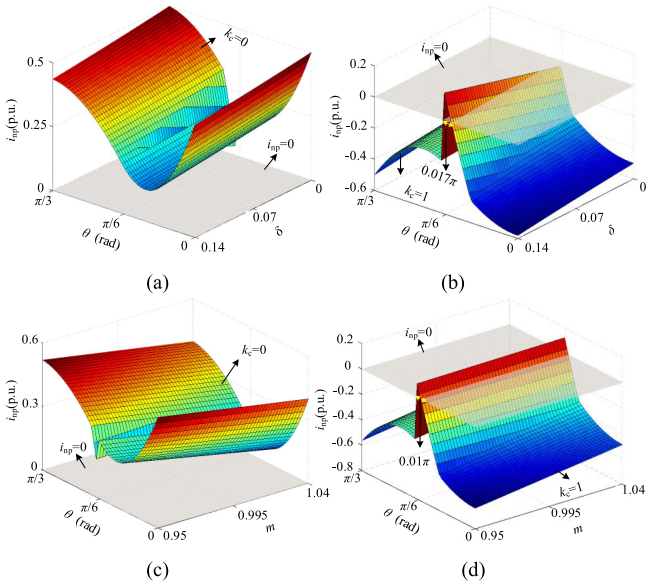

Fig. 14. NP current of DPWM under different m and δ conditions. (a) $m = 1$ and $k_c = 1$. (b) $m = 1$ and $k_c = 0$. (c) $\delta = 0.1$ and $k_c = 1$. (d) $\delta = 0.1$ and $k_c = 0$.

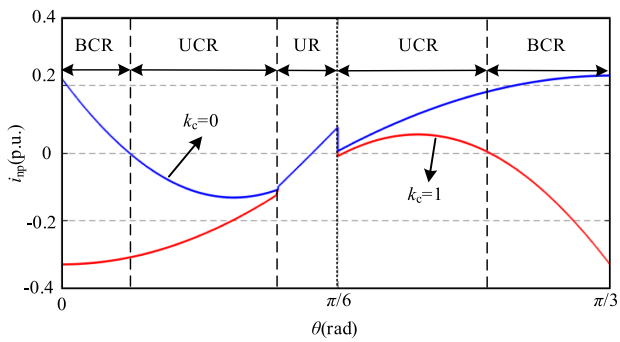

Fig. 15. NP currents corresponding to $k_c = 0$ and $k_c = 1$.

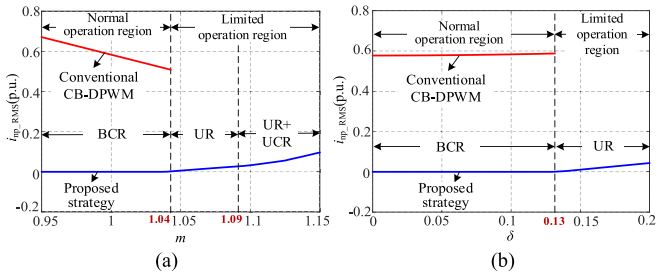

Fig. 16. RMS of NP current fluctuation with different m and δ. (a) RMS of NP current fluctuation with $\delta = 0.1$. (b) RMS of NP current fluctuation with $m = 1$.

voltage fluctuation. When the NP currents of $k_c = 0$ and $k_c = 1$ are equal, the NP voltage cannot be controlled, which is called UR. In UR, the NP voltage is uncontrollable, and there is NP voltage fluctuation. Therefore, the NP voltage fluctuation of the proposed strategy mainly occurs in UCR and UR.

In order to evaluate the NP voltage fluctuation, the root mean square (RMS) of NP current fluctuation is used, which is defined as

$$i_{\mathrm{np\_RMS}} = \frac{1}{I_{\mathrm{m}}}\left[\sqrt{\frac{1}{\varepsilon_1}\int_{\pi/6-\varphi-\varepsilon_1}^{\pi/6-\varphi} {i_{\mathrm{np0}}}^2 d\theta} + \sqrt{\frac{1}{\varepsilon_2}\int_{\pi/6}^{\pi/6+\varepsilon_2} {i_{\mathrm{np1}}}^2 d\theta} \sqrt{\frac{1}{\varphi}\int_{\pi/6-\varphi}^{\pi/6} {i_{\mathrm{np0}}}^2 d\theta}\right] \tag{33}$$

where ε_1 and ε_2 are the regions of UCR corresponding to the NP currents smaller and larger than zero, respectively. φ is the region of UR. i_{np0} and i_{np1} are the NP currents corresponding to $k_c = 0$ and $k_c = 1$, respectively.

According to (33), the RMS of NP current under different δ and m can be obtained, as shown in Fig. 16. In Fig. 16(a), when the reference voltage is in the normal operation region, the conventional CB-DPWM strategy cannot suppress the NP current fluctuation. With the increase of m, the NP voltage fluctuation

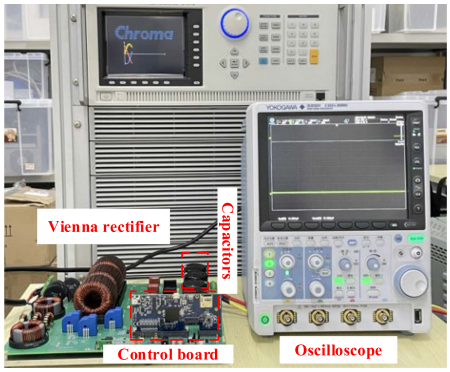

Fig. 17. Experimental platform of the Vienna rectifier.

TABLE III
PARAMETERS OF VIENNA RECTIFIER

Parameter	Value
Rated phase voltage	45 V
Input inductance	3 mH
Rated input current	4 A
Top and bottom dc-link capacitances	440 μF
Rated top and bottom dc-link resistances	15 Ω
Switching frequency	50 kHz
Grid frequency	50 Hz

decreases. At this time, the proposed strategy is in BCR, which can suppress the NP current fluctuation. With the increase of m, the proposed strategy is in the limited operation region. Due to the existence of UR and UCR, there is NP fluctuation of the proposed strategy, which is proportional to m. As can be seen from Fig. 16(b), when the reference voltage is in the normal operation region, the conventional CB-DPWM strategy has the NP current fluctuation, while the proposed strategy can minimize the NP current fluctuation. When the reference voltage is in the limited operation region, due to the existence of UR, there is the NP fluctuation of the proposed strategy, which is proportional to δ.

Therefore, the proposed strategy can minimize the NP voltage fluctuation when the reference voltage is in the normal operation region. When the reference voltage is in the limited operation region, due to the existence of UR and UCR, there is NP fluctuation of the proposed strategy, which is proportional to m and δ.

IV. EXPERIMENTAL RESULTS

The proposed strategy was verified on a Vienna rectifier experimental platform, as shown in Fig. 17. The top and bottom dc-link capacitors are connected in parallel with 440-μF electrolytic capacitors. The three-phase grid voltages are generated by the Chrome61512. The control algorithm is executed by the TMS320F28379D. To simulate different load conditions, the PO and ON of the dc link are connected to two sliding rheostats R_1 and R_2, respectively. The parameters of the Vienna rectifier are listed in Table III.

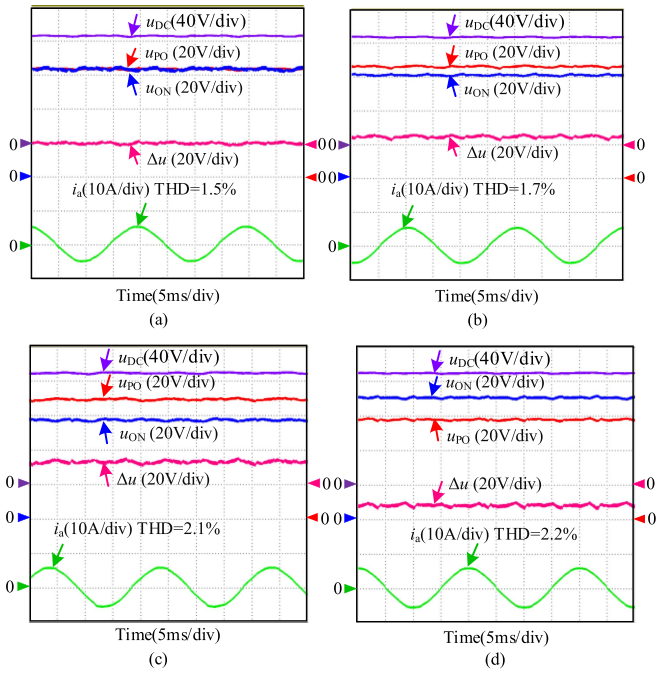

Fig. 18. Steady-state operation results of the proposed strategy under different δ. (a) $\delta = 0$. (b) $\delta = 0.03$. (c) $\delta = 0.1$. (d) $\delta = -0.1$.

Fig. 18 shows the steady-state operation results of the proposed strategy under different δ when the reference voltage is in the normal operation region. In Fig. 18(a), when $\delta = 0$, u_{po} and u_{on} of the proposed strategy can be stabilized around 63 V, and the NP voltage fluctuation is basically zero. When δ is adjusted by changing the resistance, the experimental results are as shown in Fig. 18(b)–(d). The maximum peak-to-peak value of the NP voltage Δu_{pp} under different δ is 4 V, which is 3.1% of the dc-link voltage, and the maximum total harmonic distortion (THD) of the input current is 2.2%. Therefore, the proposed strategy can reduce the NP voltage fluctuation and the input current harmonics under unbalanced dc links.

Fig. 19 shows the experimental comparison between the conventional strategy and the proposed strategy. From Fig. 19(a), when $\delta_{ref} = 0.03$ and $m = 1$, due to the influence of the NP current fluctuation, the NP voltage of the conventional strategy has a large three times grid frequency fluctuation. The peak-to-peak value of the NP voltage is 28 V, which is 22% of the dc-link voltage. When switching to the proposed strategy, it can be seen that the peak-to-peak value of the NP voltage is reduced to 3.5 V, which is 2.7% of the dc-link voltage. Therefore, the proposed strategy can minimize the NP voltage fluctuation. When $m = 1$, the maximum δ of the normal operation is 0.13, and the the corresponding Δu is 16.5 V. In Fig. 19(a), the maximum Δu of the conventional strategy and the proposed strategy is 16 V and 4 V, respectively, and the reference voltage is in the normal operation region. Therefore, the THD of the input current of the conventional strategy and the proposed strategy are basically the same, which are 2.5% and 1.7%, respectively. In Fig. 19(b), when $\delta_{ref} = 0.1$ and $m = 1$, Δu_{pp} of the conventional strategy is the same as that of Fig. 19(a) due to the same m, which is

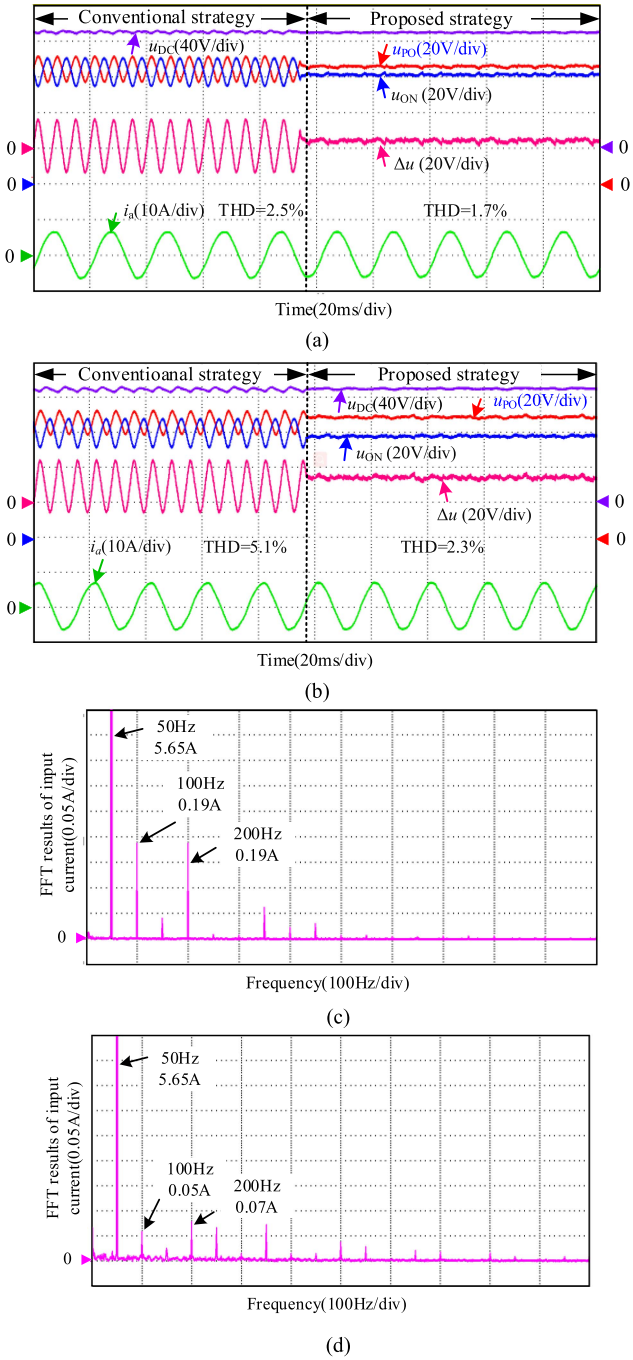

Fig. 19. Experimental comparison between the conventional and the proposed strategies. (a) $\delta_{\text{ref}} = 0.03$ and $m = 1$ (b) $\delta_{\text{ref}} = 0.1$ and $m = 1$. (c) FFT results of the conventional strategy. (d) FFT results of the proposed strategy.

22% of the dc-link voltage. When switching to the strategy proposed, Δu_{pp} is reduced to 4 V, which is 3.1% of the dc-link voltage. Due to the increase of δ, the maximum Δu of the conventional strategy is 24 V that exceeds the allowable Δu = 16.5 V of the normal operation region, which leads to the fluctuation of u_{DC} and the input current harmonics increase. Fig. 19(c) and (d) shows the FFT results of input current FFT between the two strategies when $\delta_{\text{ref}} = 0.1$ and $m = 1$. In Fig. 19(c), the input current of the conventional strategy contains

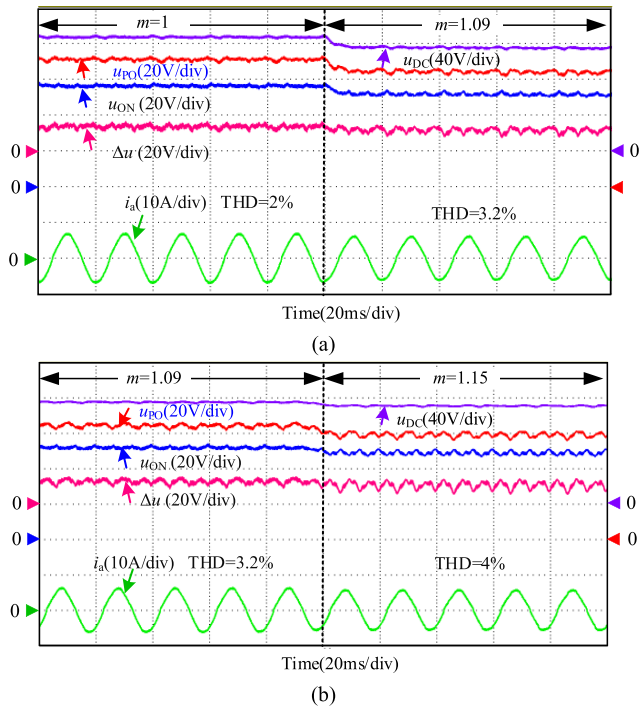

Fig. 20. Experimental results of different m with $\delta = 0.1$. (a) m from 1.04 to 1.09. (b) m from 1.09 to 1.15.

the larger second and fourth order harmonics due to the existence of the nonsynthetic subsectors. However, as can be seen from Fig. 19(d), the low-order harmonics of the input current of the proposed strategy are significantly reduced. Therefore, the proposed strategy can reduce the NP voltage fluctuation and the input current harmonics, simultaneously.

Fig. 20 shows the experimental results of different m with $\delta = 0.1$. When $\delta = 0.1$, the maximum m of the normal operation region is 1.04. As can be seen from Fig. 20(a), when $m = 1$, there is slight NP voltage fluctuation, and the input current THD is 2%. When $m = 1.09$ that exceeds 1.04, the dc-link voltage can operate stably around 116 V. However, due to the existence of UR, there is the NP voltage fluctuation at this time, and Δu_{pp} is 5 V, which is 4.3% of the dc-link voltage. The input current THD is increased to 3.2%. In Fig. 20(b), when the m increases from 1.09 to 1.15, the dc-link voltage is reduced to 112 V, and the Vienna rectifier can operate stably. Due to the influence of UR and UCR, the NP voltage fluctuation further increases, and Δu_{pp} is 8 V, which is 7.2% of the dc-link voltage. The input current THD is 4%. Therefore, when the reference voltage is in the limited operation region, the proposed strategy can still achieve stable control of the dc-link voltage, which can improve the fundamental amplitude of the output voltage under unbalanced dc links and extend the operation range of the Vienna rectifier. However, there is the NP voltage fluctuation in the limited operation region, which is proportional to m.

Fig. 21 shows experimental results of different δ with $m = 1$. When $m = 1$, the maximum δ of the normal operation region is 0.13. In Fig. 21(a), when $\delta = 0.2$ that exceeds 0.13, the dc-link voltage can operate stably around 127 V. However, due to the

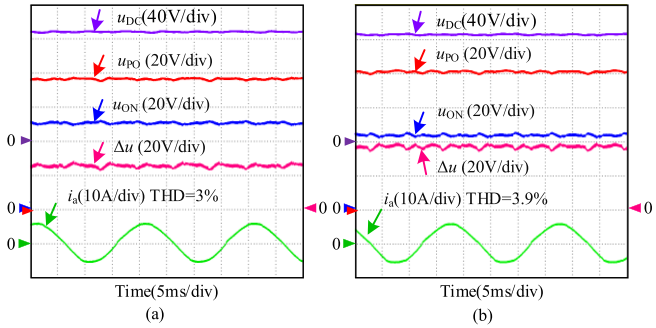

Fig. 21. Experimental results of different δ with $m = 1$. (a) $\delta = 0.2$. (b) $\delta = 0.3$.

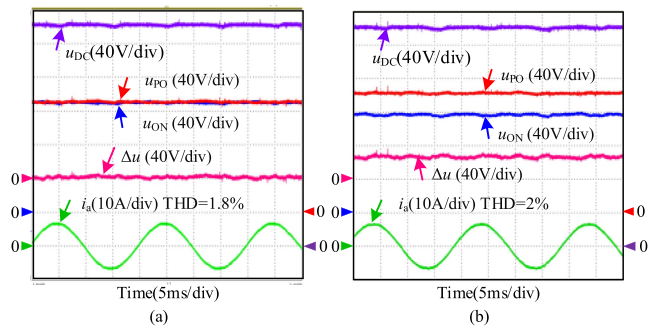

Fig. 22. Experimental results when the input phase voltage is two times rated phase voltage. (a) $\delta = 0$. (b) $\delta = 0.1$.

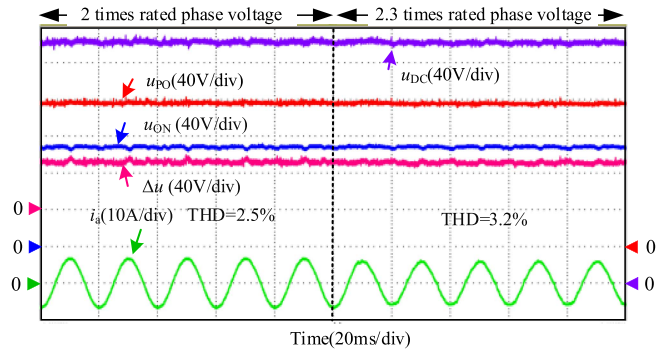

Fig. 23. Dynamic operations of the Vienna rectifier when $\delta = 0.2$.

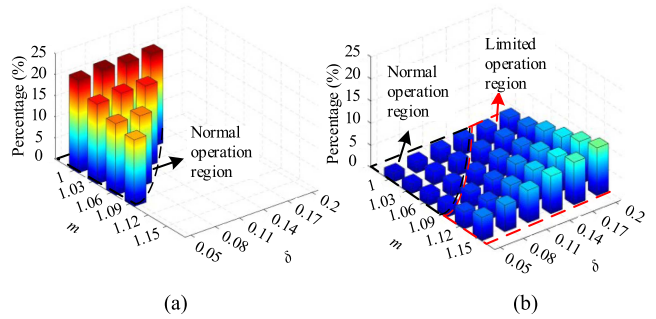

Fig. 24. Experimental results of the percentage of Δu_{pp} in dc-link voltage with different δ and m. (a) Conventional strategy. (b) Proposed strategy.

existence of UR, there is NP voltage fluctuation, and Δu_{pp} is 5.5 V, which is 4.4% of the dc-link voltage. The input current THD is 3%. From Fig. 21(b), when $\delta = 0.3$, the NP voltage fluctuation further increases due to the increase of the UR, and Δu_{pp} is 7 V, which is 5.5% of the dc-link voltage. At this time, the dc-link voltage can also operate stably around 127 V. Therefore, it further verifies that when the reference voltage is in the limited operation region, the proposed strategy can operate stably and improve the fundamental amplitude of output voltage. However, there is NP voltage fluctuation, which is proportional to δ.

Fig. 22 shows experimental results when the input phase voltage is two times rated phase voltage. In Fig. 22, the maximum peak-to-peak value of the NP voltage Δu_{pp} under different δ is 8 V, which is 3.1% of the dc-link voltage, and the maximum input current THD is 2%. As a result, the proposed strategy can operate stably with two times rated voltages, which has the same performance as the rated phase voltage.

Fig. 23 shows the dynamic operations of the Vienna rectifier when $\delta = 0.2$. As shown in Fig. 23, the dc-link voltage can operate stably around 261 V when the input phase voltages are step-up from two times to 2.3 times rated phase voltage. The maximum Δu_{pp} of the dc links is 3.1% of the dc-link voltage, and the maximum THD of the input current is 3.2%. As a result, the proposed strategy can reduce the NP voltage fluctuation and the input current harmonics during dynamic operations of the Vienna rectifier.

Fig. 24 shows the experimental results of the percentage of Δu_{pp} in dc-link voltage with different δ and m. When the reference voltage is in the normal operation region, the NP voltage fluctuation of the conventional strategy is inversely proportional to m, and the maximum is 22% of the dc-link voltage. While the maximum of the NP voltage fluctuation of the proposed strategy is 3.1% of the dc-link voltage. Therefore, the proposed strategy can minimize the NP voltage fluctuation under unbalanced dc links. When the reference voltage is in the limited operation region, the conventional strategy cannot work normally due to the limitation of the maximum m, while the proposed strategy can operate normally. There is NP voltage fluctuation of the proposed strategy, which is proportional to m and δ, and the maximum Δu_{pp} is 10.8% of the dc-link voltage.

Fig. 25 shows the experimental results of the input current THD comparison with different m and δ. When the reference voltage is in the normal operation region, the input current THD of the conventional strategy is large due to the influence of the NP voltage fluctuation, and it is inversely proportional to m and proportional to δ, whose maximum is 5.8%. While the input current THD of the proposed strategy is basically the same, whose maximum is 2.45%. When the reference voltage is in the limited operation region, the input current THD of the proposed strategy is proportional to δ and m, whose maximum is 5.5%. Therefore, the proposed strategy can simultaneously reduce the NP voltage fluctuation and the input current harmonics.

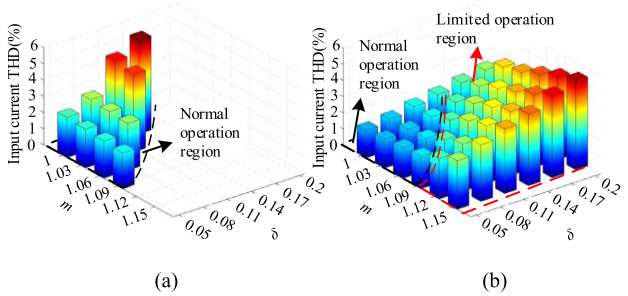

Fig. 25. Experimental results of the input current THD comparison with different m and δ. (a) Conventional strategy. (b) Proposed strategy.

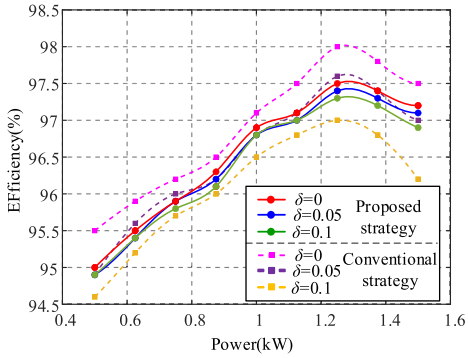

Fig. 26. Efficiency comparison of the proposed and the conventional strategies.

Fig. 26 shows the efficiency comparison of the proposed and the conventional strategies. When $\delta = 0$, the efficiency of the proposed strategy is lower than that of the conventional strategy due to the additional switching losses caused by the self-adjusting redundant clamping mode. The efficiency of the conventional strategy is inversely proportional to δ, which is caused by the NP voltage fluctuation and the input current harmonics. While the efficiency of the proposed strategy is not affected by δ. As a result, the efficiency of the proposed strategy is higher than that of the conventional strategy when $\delta = 0.1$.

V. Conclusion

An optimized CB-DPWM strategy adopting self-adjusted redundant clamping modes has been proposed in this article for Vienna rectifiers with unbalanced dc links. The operation range of the Vienna rectifier in the linear region is limited under the unbalanced dc links. The fundamental amplitude of the output voltage of the Vienna rectifier can be improved by optimizing the DPWM voltage vector trajectory. In order to reduce the NP voltage fluctuation, the redundant clamping modes are self-adjusted in real time according to the unbalanced degree. The experimental results show that when the reference voltage is in the normal operation region, the proposed strategy can reduce the NP voltage fluctuation and the harmonics of the input current. When the reference voltage is in the limited operation region, the proposed strategy can realize the stable control of the dc-link voltage, which extends the operation range of the rectifier.

References

[1] Z. He et al., "A hybrid DPWM for Vienna rectifiers based on the three-level to two-level conversion," *IEEE Trans. Ind. Electron.*, vol. 69, no. 9, pp. 9429–9439, Sep. 2022.

[2] J.-S. Lee and K.-B. Lee, "Performance analysis of carrier-based discontinuous PWM method for Vienna rectifiers with neutral-point voltage balance," *IEEE Trans. Power Electron.*, vol. 31, no. 6, pp. 4075–4084, Jun. 2016.

[3] J.-S. Lee and K.-B. Lee, "A novel carrier-based PWM method for Vienna rectifier with a variable power factor," *IEEE Trans. Ind. Electron.*, vol. 63, no. 1, pp. 3–12, Jan. 2016.

[4] W. Ding, H. Qiu, B. Duan, X. Xing, N. Cui, and C. Zhang, "A novel segmented component injection scheme to minimize the oscillation of DC-link voltage under balanced and unbalanced conditions for Vienna rectifier," *IEEE Trans. Power Electron.*, vol. 34, no. 10, pp. 9536–9551, Oct. 2019.

[5] P. Zhang, X. Wu, Z. Chen, W. Xu, J. Liu, and J. Qi, "A multi-zero-sequence component injection algorithm for a five-level flying capacitor rectifier under unbalanced DC-link voltages," *IEEE Trans. Power Electron.*, vol. 36, no. 10, pp. 11967–11983, Oct. 2021.

[6] S. Wang, N. Jiao, J. Ma, T. Liu, and X. Liu, "Analysis and optimization of voltage balancing control limits for cascaded H-bridge rectifiers," *IEEE Trans. Ind. Electron.*, vol. 68, no. 11, pp. 10677–10687, Nov. 2021.

[7] U.-M. Choi, F. Blaabjerg, and K.-B. Lee, "Control strategy of two capacitor voltages for separate mppts in photovoltaic systems using neutral-point-clamped inverters," *IEEE Trans. Ind. Appl.*, vol. 51, no. 4, pp. 3295–3303, Jul./Aug. 2015.

[8] C. Yan, D. Xu, and W. Chen, "General control scheme for a dual-input three-level inverter," *IEEE Trans. Power Electron.*, vol. 34, no. 2, pp. 1838–1850, Feb. 2019.

[9] J. Wang, S. Ji, S. Liu, H. Jiang, and W. Jiang, "A discontinuous PWM strategy to control neutral point voltage for Vienna rectifier with improved PWM sequence," *IEEE J. Emerg. Sel. Topics Power Electron.*, vol. 10, no. 3, pp. 3230–3241, Jun. 2022.

[10] L. Zhang et al., "A modified dpwm with neutral point voltage balance capability for three-phase Vienna rectifiers," *IEEE Trans. Power Electron.*, vol. 36, no. 1, pp. 263–273, Jan. 2021.

[11] S. Wang, J. Ma, B. Liu, N. Jiao, T. Liu, and Y. Wang, "Unified SVPWM algorithm and optimization for single-phase three-level npc converters," *IEEE Trans. Power Electron.*, vol. 35, no. 7, pp. 7702–7712, Jul. 2020.

[12] Y. Zou, L. Zhang, Y. Xing, Z. Zhang, H. Zhao, and Z. Zheng, "A unified carrier-based pulse width modulation for three-phase Vienna-type rectifiers," *IEEE Trans. Power Electron.*, vol. 37, no. 5, pp. 5759–5762, May 2022.

[13] L. J. Hang, B. Li, M. Zhang, Y. Wang, and L. M. Tolbert, "Equivalence of svm and carrier-based PWM in three-phase/wire/level Vienna rectifier and capability of unbalanced-load control," *IEEE Trans. Ind. Electron.*, vol. 61, no. 1, pp. 20–28, Jan. 2014.

[14] D. B. A. R. P. J. Pou, "New feedforward space-vector PWM method to obtain balanced ac output voltages in a three-level neutral-point-clamped converter," *IEEE Trans. Ind. Electron.*, vol. 49, no. 5, pp. 1026–1034, Oct. 2002.

[15] H. Wu, J. Wang, T. Liu, T. Yang, and Y. Xing, "Modified SVPWM-controlled three-port three-phase AC–DC converters with reduced power conversion stages for wide voltage range applications," *IEEE Trans. Power Electron.*, vol. 33, no. 8, pp. 6672–6686, Aug. 2018.

[16] B. Xu, K. Liu, and X. Ran, "Computationally efficient optimal switching sequence model predictive control for three-phase Vienna rectifier under balanced and unbalanced DC links," *IEEE Trans. Power Electron.*, vol. 36, no. 11, pp. 12268–12280, Nov. 2021.

[17] Z. Ye, Y. Xu, X. Wu, G. Tan, X. Deng, and Z. Wang, "A simplified PWM strategy for a neutral-point-clamped (NPC) three-level converter with unbalanced DC links," *IEEE Trans. Power Electron.*, vol. 31, no. 4, pp. 3227–3238, Apr. 2016.

[18] X. Wu, G. Tan, G. Yao, C. Sun, and G. Liu, "A hybrid PWM strategy for three-level inverter with unbalanced DC links," *IEEE J. Emerg. Sel. Top. Power Electron.*, vol. 6, no. 1, pp. 1–15, Mar. 2018.

[19] Z. He et al., "A novel method to evaluate the influence of Vienna rectifier neutral-point voltage fluctuation on input current quality," *IEEE Trans. Power Electron.*, vol. 36, no. 7, pp. 8347–8358, Jul. 2021.

[20] W. Ding, J. Liu, H. Qiu, B. Duan, and C. Zhang, "Independent voltage outputs control for Vienna rectifier considering multiple loads situations," in *Proc. IEEE 3rd Int. Future Energy Electron. Conf.*, 2017, pp. 1785–1790.

[21] W. Ding, C. Zhang, F. Gao, B. Duan, and H. Qiu, "A zero-sequence component injection modulation method with compensation for current harmonic mitigation of a Vienna rectifier," *IEEE Trans. Power Electron.*, vol. 34, no. 1, pp. 801–814, Jan. 2019.
[22] C.-Q. Xiang, C. Shu, D. Han, B.-K. Mao, X. Wu, and T.-J. Yu, "Improved virtual space vector modulation for three-level neutral-point-clamped converter with feedback of neutral-point voltage," *IEEE Trans. Power Electron.*, vol. 33, no. 6, pp. 5452–5464, Jun. 2018.
[23] X. Wu, G. Tan, Z. Ye, G. Yao, Z. Liu, and G. Liu, "Virtual-space-vector PWM for a three-level neutral-point-clamped inverter with unbalanced DC-links," *IEEE Trans. Power Electron.*, vol. 33, no. 3, pp. 2630–2642, Mar. 2018.
[24] I. M. Alsofyani and K.-B. Lee, "Simple capacitor voltage balancing for three-level npc inverter using discontinuous PWM method with hysteresis neutral-point error band," *IEEE Trans. Power Electron.*, vol. 36, no. 11, pp. 12490–12503, Nov. 2021.
[25] K. Li, M. Wei, C. Xie, F. Deng, J. M. Guerrero, and J. C. Vasquez, "Triangle carrier-based DPWM for three-level npc inverters," *IEEE J. Emerg. Sel. Topics Power Electron.*, vol. 6, no. 4, pp. 1966–1978, Dec. 2018.
[26] M. M. Hashempour, M.-Y. Yang, and T.-L. Lee, "An adaptive control of DPWM for clamped-three-level photovoltaic inverters with unbalanced neutral-point voltage," *IEEE Trans. Ind. Appl.*, vol. 54, no. 6, pp. 6133–6148, Nov./Dec. 2018.
[27] Q. Yan, L. Xiao, H. Chen, X. Yuan, H. Xu, and R. Zhao, "An analytical discontinuous space-vector PWM for three-level inverters with unbalanced DC-link voltages," *IEEE Trans. Power Electron.*, vol. 37, no. 7, pp. 7718–7728, Jul. 2022.
[28] Y. Zou et al., "Dynamic-space-vector discontinuous PWM for three-phase Vienna rectifiers with unbalanced neutral-point voltage," *IEEE Trans. Power Electron.*, vol. 36, no. 8, pp. 9015–9026, Aug. 2021.
[29] Y. Ming et al., "A hybrid carrier-based DPWM with controllable NP voltage for three-phase Vienna rectifiers," *IEEE Trans. Transp. Electrif.*, vol. 8, no. 2, pp. 1874–1884, Jun. 2022.

Zhijian Zhang received the B.S. degree in electrical engineering from the North University of China, Taiyuan, China, in 2018, and the M.S. degree from Beijing Jiaotong University, Beijing, China, in 2021. He is currently working toward the Ph.D. degree in power electronics and electrical drives with the Harbin Institute of Technology, Harbin, China.

His current research interests include permanent magnet synchronous motor control, high efficiency ac–dc converter, and Vienna rectifier control.

Binxing Li (Student Member, IEEE) received the B.S. degree in electrical engineering from the Harbin Institute of Technology, Weihai, China, in 2017. He is currently working toward the Ph.D. degree in power electronics and electrical drives with the Harbin Institute of Technology, Harbin, China.

His current research interests include permanent magnet synchronous motor drives, high efficiency ac–dc converter, and application of GaN power devices.

Guoqiang Zhang (Senior Member, IEEE) received the B.S. degree in electrical engineering from Harbin Engineering University, Harbin, China, in 2011, and the M.S. and Ph.D. degrees in electrical engineering from the Harbin Institute of Technology, Harbin, China, in 2013 and 2017, respectively.

Since 2017, he has been with the Department of Electrical Engineering, Harbin Institute of Technology, where he is currently an Associate Professor. His current research interests include control of electrical drives, and parameter identification technique, with main focus on sensorless field-oriented control of synchronous motor drives.

Dr. Zhang is an Associate Editor for the *Journal of Power Electronics*.

Gaolin Wang (Senior Member, IEEE) received the B.S., M.S., and Ph.D. degrees in electrical engineering from Harbin Institute of Technology, Harbin, China, in 2002, 2004, and 2008 respectively.

He joined the Department of Electrical Engineering, Harbin Institute of Technology as a Lecturer, in 2009, where he has been a Full Professor of electrical engineering since 2014. From 2009 to 2012, he was a Postdoctoral Fellow in Shanghai Step Electric Corporation, where he was involved in the traction machine control for direct-drive elevators. He has authored more than 100 technical papers published in journals and conference proceedings. He is the holder of ten Chinese patents. His current major research interests are ac motor drives.

Dr. Wang was a Guest Associate Editor of IEEE TRANSACTIONS ON INDUSTRIAL ELECTRONICS, an Associate Editor of IEEE ACCESS, IET Electric Power Applications, and *Journal of Power Electronics*.

Zhaobin Huang was born in Jiangxi, China, in 1986. He received the B.S. degree in control science and engineering from the College of Automation Science and Technology, Southeast University, Nanjing, China, in 2009 and the Ph.D. degree in control science and engineering from the College of Automation Science and Technology, South China University of Technology, Guangzhou, China, in 2014.

Since 2014, he has been with the R&D Center of Residential Air Conditioner Division, Midea Group. He is currently a Senior Research Engineer and the Team Leader of the Inverter-Technology. His research interests include motor drives and power electronics.

Bin Hu was born in 1988. He received the B.Eng. and Ph.D. degrees in control science and engineering from the College of Automation Science and Technology, South China University of Technology, Guangzhou, China, in 2010 and 2018, respectively.

He is currently a Research Engineer with the R&D Center of Residential Air Conditioner Division, Midea Group. His research interests include permanent magnet synchronous motor drives, power factor correction, and compressor control.

Tan Long was born in 1994. He received the B.Eng. and M.S. degrees in mechanical engineering from the Chongqing University, Chongqing, China, in 2016 and 2019, respectively.

He is currently a Research Engineer with the R&D Center of Residential Air Conditioner Division, Midea Group. His research interests include permanent magnet synchronous motor drives, power factor correction, and compressor control.

Dianguo Xu (Fellow, IEEE) received the B.S. degree in control engineering from Harbin Engineering University, Harbin, China, in 1982, and the M.S. and Ph.D. degrees in electrical engineering from Harbin Institute of Technology (HIT), Harbin, China, in 1984 and 1989, respectively.

He joined the Department of Electrical Engineering, HIT as an Assistant Professor in 1984. Since 1994, he has been a Professor with the Department of Electrical Engineering, HIT. He was the Dean of School of Electrical Engineering and Automation, HIT from 2000 to 2010. He is now the Vice President of HIT. His research interests include renewable energy generation technology, power quality mitigation, sensorless vector controlled motor drives, high performance servo system. He has published more than 600 technical papers.

Dr. Xu is an Associate Editor of the IEEE TRANSACTIONS ON INDUSTRIAL ELECTRONICS and the IEEE JOURNAL OF EMERGING AND SELECTED TOPICS IN POWER ELECTRONICS. He serves as the Chairman of IEEE Harbin Section.